
















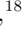






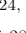























Characterization of the Host Binary of the Directly Imaged Exoplanet HD 143811 AB b

ANNE E. PECK ¹, WILLIAM ROBERSON ¹, ERIC L. NIELSEN ¹, ROBERT J. DE ROSA ², NATHALIE JONES ^{3,4},
JASON WANG ^{3,4}, BRUCE A. MACINTOSH ⁵, BRILEY L. LEWIS ⁶, GASPARD DUCHÊNE ^{7,8}, STANIMIR METCHEV ⁹,
ASIF ABAS ¹, JERRY W. XUAN ¹⁰, ANIKET SANGHI ^{11,*}, JENNIFER PATIENCE¹², TRAVIS S. BARMAN ¹³,
JOANNA BULGER ¹⁴, JEFFREY K. CHILCOTE ¹⁵, THOMAS M. ESPOSITO ^{16,17}, MICHAEL P. FITZGERALD ¹⁸,
KATHERINE B. FOLLETTE ¹⁹, HANNAH GALLAMORE ¹, STEPHEN GOODSSELL ^{20,21}, JAMES R. GRAHAM¹⁶,
ALEXANDRA Z. GREENBAUM ²², PASCALE HIBON ²³, PATRICK INGRAHAM ²³, PAUL KALAS ^{16,24,17,25},
QUINN M. KONOPACKY ²⁶, FRANCK MARCHIS ¹⁷, JÉRÔME MAIRE²⁶, CHRISTIAN MAROIS ^{27,28},
BRENDA MATTHEWS ^{29,28}, DIMITRI MAWET^{10,30}, MAXWELL A. MILLAR-BLANCHAER ⁶, REBECCA OPPENHEIMER ³¹,
DAVID W. PALMER³², MARSHALL D. PERRIN ³³, LISA POYNEER³², LAURENT PUEYO³³, ABHIJITH RAJAN ³³,
JULIEN RAMEAU ^{34,35}, FREDRIK T. RANTAKYRÖ ²¹, BIN REN ³⁶, JEAN-BAPTISTE RUFFIO ²⁶,
DMITRY SAVRANSKY ^{37,38}, ADAM C. SCHNEIDER ³⁹, ANAND SIVARAMAKRISHNAN ³³, ADAM J. R. W. SMITH ¹,
INSEOK SONG ⁴⁰, REMI SOUMMER ³³, SANDRINE THOMAS ²³, KIMBERLY WARD-DUONG ⁴¹ AND
SCHUYLER G. WOLFF ⁴²

¹Department of Astronomy, New Mexico State University, P.O. Box 30001, MSC 4500, Las Cruces, NM 88003, USA

²European Southern Observatory, Alonso de Córdova 3107, Vitacura, Casilla 19001, Santiago, Chile

³Department of Physics and Astronomy, Northwestern University, 2145 Sheridan Road, Evanston, IL 60208-3112, USA

⁴Center for Interdisciplinary Exploration and Research in Astrophysics, 1800 Sherman Ave, Northwestern University, Evanston, IL 60201, USA

⁵Department of Astronomy and Astrophysics, UC Santa Cruz, Santa Cruz CA 95064

⁶Department of Physics, University of California, Santa Barbara, CA 93106, USA

⁷Department of Astronomy, University of California, Berkeley, CA 94720, USA

⁸Univ. Grenoble Alpes/CNRS, IPAG, F-38000 Grenoble, France

⁹Department of Physics & Astronomy, Institute for Earth and Space Exploration, The University of Western Ontario, London, ON N6A 3K7, Canada.

¹⁰Department of Astronomy, California Institute of Technology, Pasadena, CA 91125, USA

¹¹Cahill Center for Astronomy and Astrophysics, California Institute of Technology, 1200 E. California Boulevard, MC 249-17, Pasadena, CA 91125, USA

¹²School of Earth and Space Exploration, Arizona State University, Tempe, AZ 85287, USA

¹³Lunar and Planetary Lab, University of Arizona, Tucson, AZ 85721, USA

¹⁴Institute for Astronomy, University of Hawai'i, 2680 Woodlawn Drive, Honolulu, HI 96822, USA

¹⁵Department of Physics and Astronomy, University of Notre Dame, 225 Nieuwland Science Hall, Notre Dame, IN, 46556, USA

¹⁶Department of Astronomy, 501 Campbell Hall, University of California Berkeley, Berkeley, CA 94720-3411, USA

¹⁷SETI Institute, Carl Sagan Center, 339 Bernardo Ave Ste 200, Mountain View, CA 94043, USA

¹⁸Department of Physics & Astronomy, University of California, Los Angeles, CA 90095, USA

¹⁹Physics and Astronomy Department, Amherst College, 25 East Drive, Amherst, MA 01002, USA

²⁰Department of Physics, Durham University, Stockton Road, Durham DH1, UK

²¹Gemini Observatory, Casilla 603, La Serena, Chile

²²IPAC, Mail Code 100-22, Caltech, 1200 E. California Blvd., Pasadena, CA 91125, USA

²³Vera C. Rubin Observatory, 950 N Cherry Ave, Tucson AZ, 85719, USA

²⁴SETI Institute, Carl Sagan Center, Mountain View, CA 94043, USA

²⁵Institute of Astrophysics, FORTH, GR-71110 Heraklion, Greece

²⁶Department of Astronomy & Astrophysics, University of California San Diego, La Jolla, CA, USA

²⁷National Research Council of Canada Herzberg, 5071 West Saanich Rd, Victoria, BC, V9E 2E7, Canada

²⁸Department of Physics & Astronomy, University of Victoria, 3800 Finnerty Rd., Victoria, BC V8P 5C2, Canada

²⁹Herzberg Astronomy and Astrophysics, National Research Council of Canada, 5071 West Saanich Rd., Victoria, BC V9E 2E7, Canada

³⁰Jet Propulsion Laboratory, California Institute of Technology, 4800 Oak Grove Drive, Pasadena, CA 91109, USA

³¹American Museum of Natural History, Department of Astrophysics, Central Park West at 79th Street, New York, NY 10024, USA

³²Lawrence Livermore National Laboratory, 7000 East Avenue, Livermore, CA, 94550, USA

³³Space Telescope Science Institute, 3700 San Martin Drive, Baltimore, MD 21218, USA

³⁴Trottier Institute for Research on Exoplanets, Université de Montréal, Département de Physique, C.P. 6128 Succ. Centre-ville, Montréal, QC H3C 3J7, Canada

³⁵University of Grenoble Alpes, CNRS, IPAG, F-38000 Grenoble, France

³⁶Observatoire de la Côte d’Azur, 96 Bd de l’Observatoire, 06304 Nice, France

³⁷Sibley School of Mechanical and Aerospace Engineering, Cornell University, Ithaca, NY 14853, USA

³⁸Propulsion Laboratory, California Institute of Technology, 4800 Oak Grove Dr., Pasadena, CA 91109, USA

³⁹United States Naval Observatory, Flagstaff Station, 10391 West Naval Observatory Road, Flagstaff, AZ 86005, USA; Department of Physics and Astronomy, George Mason University, MS3F3, 4400 University Drive, Fairfax, VA 22030, USA

⁴⁰Department of Physics and Astronomy, University of Georgia, Athens, GA 30602, USA

⁴¹Department of Astronomy, Smith College, Northampton, MA, 01063, USA

⁴²Steward Observatory, University of Arizona, Tucson, AZ 85721, USA

ABSTRACT

HD 143811 AB is the host star to the directly imaged planet HD 143811 AB b, which was recently discovered using data from the Gemini Planet Imager and Keck NIRC2. A member of the Sco-Cen star-forming region with an age of 13 ± 4 Myr, HD 143811 AB is somewhat rare among hosts of directly imaged planets as it is a close stellar binary, with an ~ 18 day period. Accurate values for the orbital and stellar parameters of this binary are needed to understand the formation and evolutionary history of the planet in orbit. We utilize archival high-resolution spectroscopy from FEROS on the MPG/ESO 2.2-meter telescope to fit the orbit of the binary, and combine with unresolved photometry to derive the basic stellar properties of the system. From the orbit, we derive precise values of orbital period of 18.59098 ± 0.00007 days, and mass ratio of 0.885 ± 0.003 . When combined with stellar evolutionary models, we find masses of both components of $M_A = 1.30^{+0.03}_{-0.05} M_\odot$ and $M_B = 1.15^{+0.03}_{-0.04} M_\odot$. While the current data are consistent with the planet and stellar orbits being coplanar, the 3D orientations of both systems are currently poorly constrained, with additional observations required to more rigorously test for coplanarity.

Keywords: Binary stars, Planet hosting stars, Exoplanets, Spectroscopic binary stars

1. INTRODUCTION

A vital part of studying exoplanets is understanding their stellar hosts. The key parameter of age, especially important for self-luminous planets, is more readily measured from the host star than the planet, especially if the star is part of a moving group or association (e.g. [A. M. Lagrange et al. 2010](#), [J. Rameau et al. 2013](#), [J. Gagné et al. 2018](#)). The mass of the star is also of great interest, both to constrain orbital motion (e.g. [R. J. De Rosa et al. 2015](#)) and to determine how exoplanet occurrence rate depends on stellar mass (e.g. [J. A. Johnson et al. 2010](#); [E. L. Nielsen et al. 2019](#)).

Exoplanets in binary (and other multiple) systems represent a particularly interesting dataset. Typically, single stars are targeted by exoplanet surveys given observational constraints; however, some binary configurations still allow for planet detection. In the case of direct imaging, exoplanets have been identified orbiting a single star in a multiple system (e.g. 51 Eri b, [B. Macintosh et al. 2015](#)) as well as circumbinary planets orbiting far from an inner binary (e.g. HD 106906 b, [V. Bailey et al. 2014](#)). In addition to providing constraints on planet formation (e.g. [A. L. Kraus et al. 2016](#)), these planetary systems are also more likely to experience complex 3-body dynamics, such as Kozai-Lidov oscillations (e.g. [A. Cheetham et al. 2018](#)).

Using Gemini-South/GPI and Keck/NIRC2 data, a giant exoplanet was recently confirmed to be orbiting the binary star HD 143811 AB (HIP 78663). The planet is at a separation of ~ 59 au and has a mass of $\sim 5.6 M_{\text{Jup}}$ ([N. Jones et al. 2025](#), submitted ApJL). In this work we characterize the stellar binary host using a new analysis of archival and catalog data. We combine a new orbit fit with SED fitting of the system to derive the individual masses and orbital

* NSF Graduate Research Fellow

properties of the binary, in order to understand HD 143811 AB b in the broader context of planet formation within both single stars and binaries.

2. HD 143811 AB

HD 143811 AB, before being determined to be a binary, was identified as a member of the Sco-Cen star forming region (P. T. de Zeeuw et al. 1999). In particular, the star was assigned to Upper Scorpius by P. T. de Zeeuw et al. (1999), M. J. Pecaut et al. (2012), and P. A. B. Galli et al. (2018). K. L. Luhman & T. L. Esplin (2020), however, rejected HD 143811 AB as an Upper Sco member when conducting an Upper Sco census based on *Gaia* DR2 data (Gaia Collaboration et al. 2018), instead classifying it as part of “the remainder of Sco-Cen.” This detailed membership analysis was based on UVW velocities utilizing *Gaia* DR2 proper motions and parallax and, in the case of HD 143811 AB, a radial velocity of $RV = -11.3 \pm 0.3$ km/s from C. H. Chen et al. (2011). Given our analysis below, this radial velocity measurement likely captured the binary orbital motion, shifting the measurement of U from its true value by ~ 10 km/s.

BANYAN Σ (J. Gagné et al. 2018) gives a 69.5% chance that HD 143811 AB is a member of Upper Sco, a 30.3% chance of being part of UCL (Upper Centaurus-Lupus), and a 0.2% chance of being in the field. This analysis is based on *Gaia* DR3 (Gaia Collaboration et al. 2023) parallax and proper motion and the DR2 (Gaia Collaboration et al. 2018) radial velocity (1.68 ± 0.96 km/s). Substituting the system radial velocity we derive below (0.48 ± 0.02 km/s) we find similar probabilities, but with a slightly higher chance of Upper Sco membership: 72.1%, compared to 27.8% and 0.2% chances of UCL and the field, respectively.

Given ages of Upper Sco of 10 ± 3 Myr and UCL of 16 ± 2 Myr (M. J. Pecaut et al. 2012), and the uncertainty in the subgroup membership, we adopt an age for the system of 13 ± 4 Myr. This is consistent with the 2D age map of M. J. Pecaut & E. E. Mamajek (2016), where ages between ~ 10 –17 Myr are close to the 2D location of HD 143811 AB. HD 143811 AB was also identified as hosting a debris disk from detections of an infrared excess (e.g. C. H. Chen et al. 2011).

More recently, HD 143811 AB was identified as a spectroscopic binary from analysis of high resolution spectroscopy. O. V. Zakhzhay et al. (2022) obtained 15 epochs of FEROS spectra, and note the target is a double lined spectroscopic binary (SB2) with a period between 20-80 days with a companion mass in the stellar regime. We utilize these archival FEROS data, as well as archival spectra from additional epochs, below in our analysis of the system. Similarly, A. Grandjean et al. (2023) obtain three HARPS (High Accuracy Radial velocity Planet Searcher) spectra of the system within one day, noting the cross-correlation function of HD 143811 AB is double-peaked, suggesting a stellar binary.

3. DATA

HD 143811 AB was observed by the MPG/ESO 2.2-meter telescope/FEROS (Fiber-fed Extended Range Optical Spectrograph, A. Kaufer et al. 1999) on 22 epochs between 17 Apr 2018 and 18 Apr 2022. These $R \sim 48,000$ spectra clearly show two sets of stellar lines, identifying the system as an SB2, and in many epochs the two sets of lines are clearly separated. At other epochs, near conjunction, the velocities of the two stars are more comparable, and the lines overlap. The combination of multiple years of coverage and the ~ 1 day cadence of many observations allows excellent time sampling of the orbital motion. Since FEROS obtains spectra of both the science target and a wavelength calibration lamp simultaneously, the spectra have exceptional wavelength stability with radial velocity precision as low as ~ 6 m/s (O. V. Zakhzhay et al. 2022). We retrieve the reduced spectra from the ESO Phase 3 archive.

4. ANALYSIS

We use the FEROS spectra to derive physical and orbital properties of the HD 143811 AB binary system and the individual stars.

4.1. Spectral Fitting

The two stellar components of HD 143811 AB are near equal brightness, and are close enough (~ 1 mas) that the data contain combined spectra of both stars in all epochs. Nevertheless, the large RV semi-amplitude of each star in the system (~ 25 km/s) and the high spectral resolution of FEROS result in significant separation of spectral lines at some epochs.

We extract velocities and parameters for each star by generating a model of the combined spectrum and comparing to the observations, using a grid of PHOENIX stellar atmosphere models (P. H. Hauschildt & E. Baron 1999) from

T. O. Husser et al. (2013). We explore the parameter space of the model with Markov Chain Monte Carlo (MCMC) as implemented in the *emcee* package (D. Foreman-Mackey et al. 2013). Our model consists of 11 parameters: RV offsets for both the primary and the secondary, effective temperature for both components, $\log(g)$ for both components, $v\sin(i)$ for both components, system metallicity, a single flux ratio between the two stars, and an additional broadening parameter σ . This last term accounts for resolution differences between FEROS and PHOENIX, but also broadening due to atmospheric seeing. The PHOENIX grid is linearly interpolated in effective temperature, metallicity, and $\log(g)$, generating two spectra, one for each component of the binary. The resolution of the PHOENIX template is degraded to match that of the FEROS spectra using a Gaussian kernel with a width set to σ , and the model spectrum is further broadened using a $v\sin(i)$ kernel. Next, we scale the model spectrum for the B component using the flux ratio and then combine the two spectra before normalizing to the continuum level of the data. We perform the fit on 9 regions ($\sim 3\text{--}8\text{ \AA}$ in width) of the spectrum with well-modeled narrow lines (mostly Fe I and Fe II lines) between 6,000 and 8,000 \AA . Error bars are assigned to each spectral channel based on the channel-to-channel variation seen in continuum regions, and then inflated by a factor of two to account for spectral covariance and model mismatch. Our final error bars are about 3% for each spectral channel.

For eleven epochs where the two sets of lines are well-separated ($\Delta RV \gtrsim 20\text{ km/s}$), we perform a fit with uniform priors in $v\sin(i)$, RV, T_{eff} , metallicity, and σ . These broad priors have $-50\text{ km/s} \leq RV \leq 50\text{ km/s}$, $4000\text{ K} \leq T_{\text{eff}} \leq 8000\text{ K}$, $1\text{ km/s} \leq v\sin(i) \leq 10\text{ km/s}$, $-0.5 \leq Z \leq 0.5$, $0.1 \leq \text{FR} \leq 1.0$, and $0.01 \leq \sigma \leq 100$. Since our method does not reliably fit $\log(g)$ (see Appendix), we select priors for $\log(g)$ of each star based on the grids from I. Baraffe et al. (2015) for 10-20 Myr stars at $1.3M_{\odot}$ and $1.15M_{\odot}$. We use Gaussian priors on $\log(g)$ of 4.1 ± 0.1 and 4.2 ± 0.1 for the primary and secondary, respectively. As expected, the posteriors on $\log(g)$ match the priors. An example of the posterior distributions for each parameter for one epoch is presented in the Appendix in Figure 6.

While the parameters derived from each epoch generally agree, final T_{eff} , $v\sin(i)$, and metallicity are calculated from the summed 1D posteriors across these nine epochs, to better incorporate systematic errors. Error bars are taken to be the standard deviations of the combined posterior added in quadrature to 56.9 K and 0.052 dex in temperature and metallicity. The derivation of these additional error terms, from a comparison of our method to literature results on 10 stars, is presented in the Appendix. Stellar parameters are given in Table 1, and Figure 1 shows an example segment of the spectrum, with FEROS data in black, and fits in red. Overall there is good agreement between model and data, though as expected there are mismatches between the model and data for some lines.

For epochs where the relative RVs are smaller than 20 km/s (11 epochs) and the lines mostly overlap, using wide priors results in poor fits with degeneracies between the multiple parameters. While these epochs are not suitable for additional measurements of the stellar parameters, they can still be used to extract RVs of both stars. For the epochs with more overlapping lines we use narrower priors, based on the fit results to epochs with more separated lines. While the radial velocity prior remains $-50\text{ km/s} \leq RV \leq 50\text{ km/s}$, we adjust the priors for the other parameters for the overlapping epochs. We adopt Gaussian priors from our adopted posteriors on the stellar parameters, based on the fitting to epochs with more widely-separated lines. The measured RVs for each epoch are reported in Table 2.

As expected for young F-stars we detect significant lithium absorption in both stars near 6707.8 \AA . We do not observe significant emission cores in Calcium H and K or in $H\alpha$.

4.2. Orbit Fitting

We perform an orbit fit (using the same Metropolis-Hastings MCMC method as E. L. Nielsen et al. 2020) to the SB2 based on our measured velocities, fitting for the RV semi-amplitude of both stars, period, eccentricity, argument of periastron, epoch of periastron passage, and system RV. Uniform priors are assumed on all parameters, with eccentricity bounded between $0 \leq e \leq 0.95$. Ten MCMC chains are run in parallel for 10^7 steps each, with every 100th step saved. We assess convergence both by visual inspection of the posteriors and by considering the Gelman-Rubin statistics, which is below 1.001 for all parameters. Since the data contain both high-cadence observations (15 epochs over two weeks) and long baselines (four years between the first and last epoch) the constraints on the orbital parameters are excellent.

Figure 2 shows the RVs of both components and draws from the posterior. The best-fitting orbit has a reduced χ^2 close to unity, indicating our RV error bars are appropriate. The posteriors on this fit are shown in Figure 3. Period is constrained to approximately six seconds: $P = 18.59098 \pm 0.00007$ days, and mass ratio constrained to less than a percent: $q = 0.885 \pm 0.003$. The significant eccentricity of the orbit is well-determined, $e = 0.4935 \pm 0.0013$, and the $\sim 90\%$ mass ratio is consistent with the similarity of the two spectra, as well as the similar depths of the lines.

Table 1. Properties of HD 143811 AB

Parameter	HD 143811 A	HD 143811 B	Reference
Age (Myr)	13 ± 4		1
Distance (pc)	136.9 ± 0.4		2
<i>Spectral Fitting</i>			
Metallicity	−0.18 ± 0.10		1
T _{eff} (K)	6439 ± 132	5900 ± 157	1
v sin(<i>i</i>) (km/s)	6.8 ± 0.6	2.8 ± 1.4	1
<i>Orbit Fitting</i>			
<i>K</i> (km/s)	22.76 ± 0.05	25.71 ± 0.06	1
Period (days)	18.59098 ± 0.00007		1
Eccentricity	0.4935 ± 0.0013		1
ω (deg)	155.91 ± 0.18	335.91 ± 0.18	1
T ₀ (MJD)	58230.438 ± 0.006		1
RV ₀ (km/s)	0.48 ± 0.02		1
$q = \frac{M_B}{M_A}$	0.885 ± 0.003		1
<i>SED Fitting</i>			
[<i>M/H</i>] (dex)	−0.15 ^{+0.07} _{−0.08}		1
Age (Myr)	20.9 ^{+1.8} _{−1.7}		1
A _V (mag)	0.16 ± 0.01		1
T _{eff} (K)	6751 ⁺²⁰⁷ _{−148}	6349 ⁺¹²² _{−133}	1
Mass (M _⊙)	1.30 ^{+0.03} _{−0.05}	1.15 ^{+0.03} _{−0.04}	1
<i>Combined Results</i>			
Semi-major axis (AU)	0.1854 ^{+0.0014} _{−0.0024}		1
Inclination Angle (deg)	22.9 ^{+0.3} _{−0.2}		1

References—1: this work, 2: [Gaia Collaboration et al. \(2023\)](#)

4.3. Stellar Parameters

The SB2 orbit does not provide direct measurements of the individual masses, semi-major axis, or inclination angle. Nevertheless, with the mass ratio and unresolved photometry of the system, we can derive model-dependent values of these parameters. We follow the same procedure outlined in [E. L. Nielsen et al. \(2019\)](#) for stars with $B - V > 0.35$, using a joint evolutionary-atmospheric model to fit the blended photometry of the system to estimate the masses of the two components. As in [E. L. Nielsen et al. \(2019\)](#), we use a modified version of the MESA Isochrones and Stellar Tracks (MIST) model grid ([A. Dotter 2016](#); [J. Choi et al. 2016](#)) combined with ATLAS9 model atmospheres ([F. Castelli & R. L. Kurucz 2003](#)). With this approach, we can estimate the spectral energy distribution (SED) of the two stars given the masses of the two components (M_1 , M_2) and an age (t), metallicity ($[M/H]$), parallax (ϖ), extinction (A_V) for the system. The joint evolutionary-atmospheric model allows us to translate these parameters into the observable SED of the system, the two components being unresolved and blended together due to their very small angular separation. This can then be used to fit the observed optical photometry from *Gaia* ([Gaia Collaboration et al. 2023](#)) and near-infrared photometry from 2MASS ([M. F. Skrutskie et al. 2006](#)). While this system has a debris disk, the observed excess is at ~ 24 microns, and so the disk should not impact the bluer photometry. The observed and modeled SED is shown in Figure 4, while the triangle plot for this fit is given in the Appendix in Figure 7.

Table 2. Radial Velocities of HD 143811 A and B.

Epoch (MJD)	RV _A (km/s)	RV _B (km/s)
58225.34288748	12.47 ± 0.12	−13.37 ± 0.13
58226.33491006	11.4 ± 0.12	−11.47 ± 0.14
58227.32819053	8.05 ± 0.13	−8.29 ± 0.15
58228.32557202	1.85 ± 0.33	−1.11 ± 0.39
58228.41252391	1.3 ± 0.42	−0.42 ± 0.49
58229.39170289	−12.04 ± 0.13	14.43 ± 0.13
58230.37940065	−29.89 ± 0.12	34.72 ± 0.13
58231.36509343	−29.44 ± 0.12	34.19 ± 0.13
58233.33550644	−9.64 ± 0.12	11.86 ± 0.13
58235.34602336	1.34 ± 0.36	−0.48 ± 0.4
58236.20482821	3.77 ± 0.23	−3.59 ± 0.21
58236.27410678	4.2 ± 0.22	−3.63 ± 0.19
58236.36759109	4.32 ± 0.22	−4.12 ± 0.18
58237.37519999	7.34 ± 0.16	−6.64 ± 0.17
58238.35257748	8.86 ± 0.13	−9.02 ± 0.13
59432.07530098	13.01 ± 0.12	−13.37 ± 0.13
59435.13101458	10.19 ± 0.13	−10.83 ± 0.13
59438.08030089	−17.2 ± 0.12	20.55 ± 0.15
59682.31235944	−19.76 ± 0.12	23.54 ± 0.14
59684.30321624	−3.89 ± 0.21	5.67 ± 0.22
59687.27883468	6.62 ± 0.17	−6.2 ± 0.18
59690.32627126	11.36 ± 0.13	−12.11 ± 0.14

With our combined model in hand, we use an MCMC-based approach for parameter estimation. We use Gaussian priors for the age ($t = 13 \pm 4$ Myr; synthesizing the age for the US and UCL sub-groups from [M. J. Pecaut & E. E. Mamajek 2016](#)), parallax ($\varpi = 7.3065 \pm 0.0204$ mas; [Gaia Collaboration et al. 2023](#)), metallicity ($[M/H] = -0.05 \pm 0.11$ dex; [E. L. Nielsen et al. 2013](#)), and mass ratio ($q = 0.885 \pm 0.003$). From this, we find individual masses of the two stars of $M_A = 1.30^{+0.03}_{-0.05} M_\odot$ and $M_B = 1.15^{+0.03}_{-0.04} M_\odot$, although the two masses are highly covariant given the tight constraint on the mass ratio.

Based on the sum of these individual masses and the orbital period, we find a semi-major axis (for the orbit of B around A) of $0.1854^{+0.0014}_{-0.0024}$ au. Combined with the eccentricity of the orbit and the distance to the system, apastron should be ~ 2 mas. While this is too close for traditional imaging, it should be reachable with an interferometer like VLTI/GRAVITY ([GRAVITY Collaboration et al. 2017](#)). This semi-major axis is a factor of ~ 300 smaller than the planet separation; such a large difference would be expected for a stable orbit of a planet around a binary star.

We also use the posteriors on velocity semi-amplitude of both components, the period, and the eccentricity, as well as the inferred masses and uncertainties from the SED fitting, to derive the inclination angle. As expected for self-consistent results, both semi-amplitudes return similar values of inclination angle: $i_A = 22.9^{+0.3}_{-0.2}^\circ$ and $i_B = 22.8^{+0.3}_{-0.2}^\circ$. We adopt the first value as the model-dependent inclination angle of the system. Since radial velocity measurements cannot distinguish between clockwise and counterclockwise orbits, a value of $i = 156.1^{+0.2}_{-0.3}^\circ$ is also possible.

5. DISCUSSION

5.1. Physical Parameters

The relatively large eccentricity of HD 143811 AB (~ 0.5) is not unexpected given the orbital period of ~ 18 days. [G. Torres et al. \(2021\)](#), examining Pleiades binaries, find that tidal circularization is most prominent for orbital periods below ~ 7 days. The binary period itself is typical of FGK binaries, though the peak of the distribution is closer to 10^5 days (~ 300 years), the log-normal distribution is quite broad ([A. Duquennoy & M. Mayor 1991](#), [D. Raghavan](#)

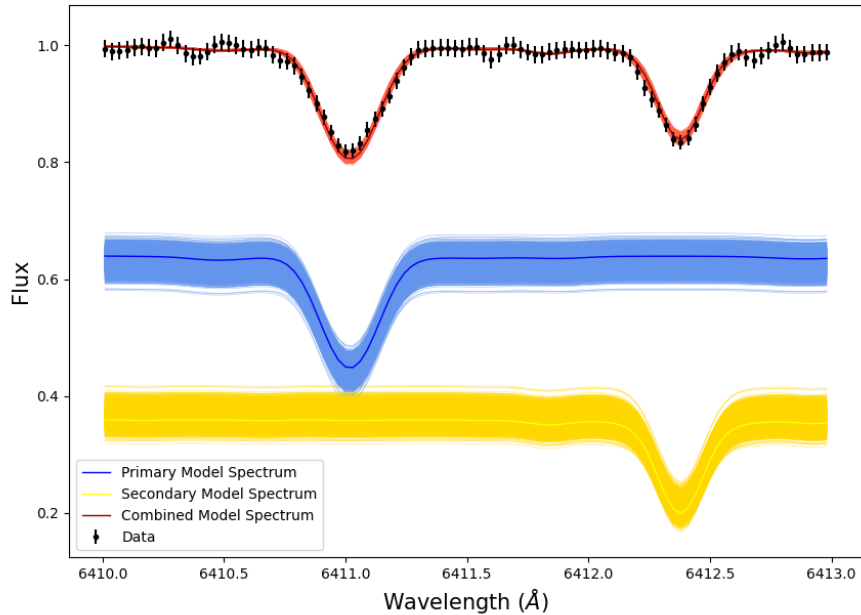


Figure 1. FEROS spectrum of HD 143811 AB taken on 2018-04-18 (black points with error bars), showing two sets of well-resolved lines. Red tracks are draws from the posterior (lowest chi-square solution in dark red) of a two-star model that best fits the data. The blue and yellow lines are draws from single star models for A and B, respectively. Given the high resolution and SNR of these data we are able to recover both the radial velocities of both components as well as individual stellar parameters.

et al. 2010). The discovery of a planet around such a binary is partially the result of an important selection effect: wider-separation binaries (~ 0.1 ”) would be excluded from the GPIES target list, or aborted once the binary became visible. This is due both to the expected lack of dynamical space for a planet with similar orbital separation to a stellar binary, and the practical effect that a star not occulted by the coronagraph would saturate the detector. As a result, binary stars identified as planet hosts by direct imaging surveys tend to either have very small orbits (so that both stars fit comfortably under the coronagraph), or very large orbits (so that the other star is well outside the field of view of the detector).

There is a significant offset between the temperatures we derive for the two components from fitting the SB2 spectrum (6439 ± 132 and 5900 ± 157 K) compared to fitting the SED and the mass ratio (6751^{+207}_{-148} and 6349^{+122}_{-133} K). The SED results are systematically ~ 300 K higher than the spectral fitting results; the $\sim 1 \sigma$ confidence intervals touch for HD 143811 A, while the confidence intervals touch at $\sim 1.5 \sigma$ for HD 143811 B. In the SED fit, there is a strong covariance between the extinction and both temperatures, with lower values of extinction corresponding to lower temperatures. There is a range of extinction values across Sco-Cen, both across subgroups (the mean A_V is 0.73 and 0.17 for Upper Sco and UCL, respectively, E. J. de Geus et al. 1989; N. J. Wright & E. E. Mamajek 2018) and within subgroups. M. J. Pecaut & E. E. Mamajek (2016), for example, find multiple members of both Upper Sco and UCL with large extinctions ($A_V \sim 1$), as well as stars with extinctions as low as $A_V = 0$. Setting the extinction in the SED fit to $A_V = [0.00, 0.05, 0.10]$ moves the median temperatures of A and B to $[6530, 6564, 6636]$ K and $[6104, 6216, 6297]$ K, respectively; the lowest of these values are more in line with the spectral fitting results.

Alternatively, there may be a systematic offset in the spectral fitting when fitting an SB2 compared to fitting single stars. A significant issue is the incompleteness of models, especially lines that appear in the model but not the data or vice versa. These are visible when comparing either FEROS or APO/ARCES data to the PHOENIX models, and we chose the spectral regions for the fit to isolate well-modeled lines. However, this can become more important when the RV offset of an SB2 results in a well-modeled line in one star overlaps with a poorly-modeled line in the other.

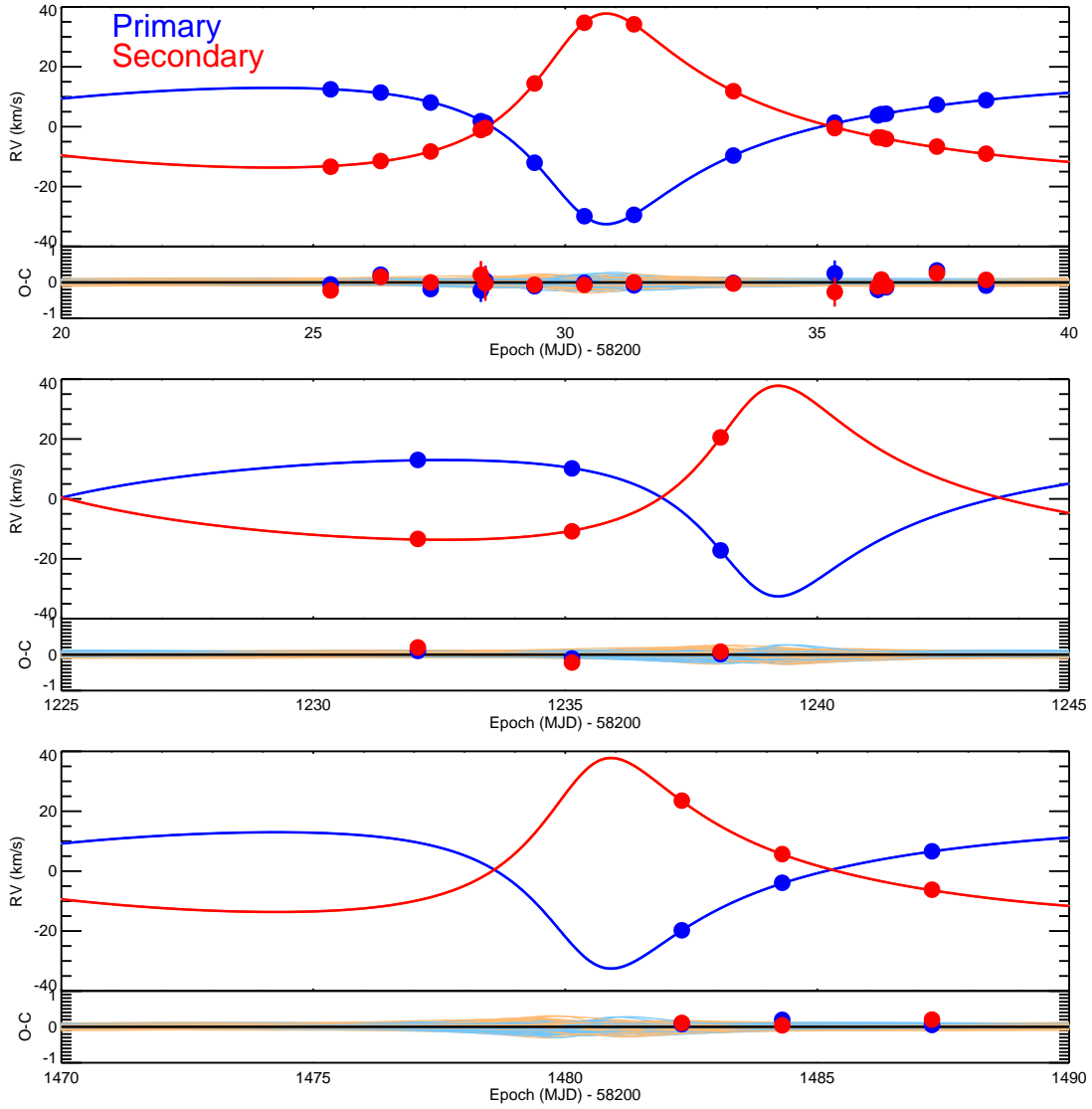


Figure 2. Radial velocity measurements of both HD 143811 A and HD 143811 B with orbits drawn from the posteriors, with the darkest blue and red lines representing the lowest χ^2 orbit. The Observed-Computed (O-C) panels show the residuals with respect to the lowest χ^2 orbit (black line at 0), as well as the offset of other draws from the posterior with respect to the best-fitting orbit. The ~ 18 day orbit is an excellent fit to the data, and the combination of multiple observation over 2 weeks and a multi-year baseline strongly constrain the orbital parameters.

While the masses of the two components have some covariance with temperature in the SED fit, this effect is relatively small. As a result, our derived masses of the two components ($1.30^{+0.03}_{-0.05}$ and $1.15^{+0.03}_{-0.04} M_{\odot}$) are generally better constrained than the temperatures.

5.2. Debris Disk

HD 143811 AB likely contains a cold debris belt, based on measurements of an IR excess. C. H. Chen et al. (2011) measured a 7.8σ infrared excess at $24 \mu\text{m}$ for HD 143811 AB, based on *Spitzer* data, though note that there is some contamination in the photometric measurement. The archival *Spitzer* $24\mu\text{m}$ data shows a point-like source for this object, suggesting the level of contamination is minimal. N. P. Ballering et al. (2013) also concludes there is a cold debris belt from the *Spitzer* IR excess. Follow-up analysis by C. H. Chen et al. (2014) combines MIPS data with IRS spectra, and does not mention contamination for this source. C. H. Chen et al. (2014) find excesses of 2%, 38%, and 25% at 13, 24, and $31 \mu\text{m}$, respectively, with a non-detection (of both the star and the disk) at $70 \mu\text{m}$.

The reported fractional IR luminosity of the system varies by almost an order of magnitude between datasets used and analysis techniques. C. H. Chen et al. (2011) use the *Spitzer* photometric excess to calculate a fractional IR

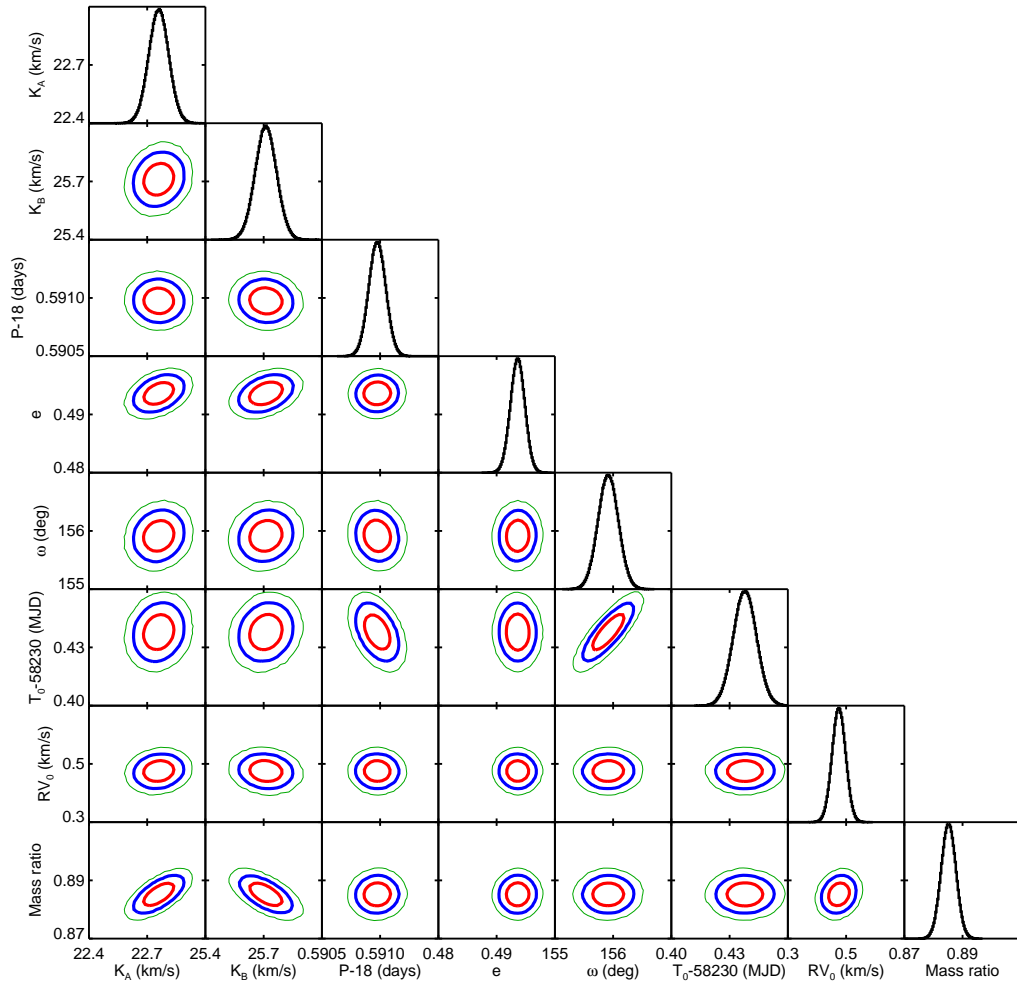


Figure 3. Posterior on the SB2 radial velocity orbit of HD 143811 AB. The orbit is very well constrained by the FEROS data, with orbital period known to 10 second precision. Direct measurement of both semi-amplitudes allows a measurement of mass ratio at the sub-1% level: 0.885 ± 0.003 .

luminosity of $\frac{L_{IR}}{L_*} = 3.8 \times 10^{-5}$. A higher luminosity of $1.1^{+0.2}_{-0.1} \times 10^{-4}$ is found by C. H. Chen et al. (2014) when including *Spitzer* IRS data, while H. Jang-Condell et al. (2015) found a lower value of 3.3×10^{-5} based on these same data. I. McDonald et al. (2012) combines multiple photometric measurements, including ALLWISE (E. L. Wright et al. 2010), deriving an even higher fractional luminosity of 2.411×10^{-4} . T. H. Cotten & I. Song (2016) combines *Spitzer* and ALLWISE data, finding $\frac{L_{IR}}{L_*} = 0.84 \times 10^{-4}$.

The inferred disk parameters vary as well between authors. T. H. Cotten & I. Song (2016) find a disk with a temperature of 140 K and a radius of 8.5 au. C. H. Chen et al. (2011) and C. H. Chen et al. (2014) find cooler temperatures of 68 and 100 K, with a further-out disk radius of 90 and 23.8 au, respectively. Alternatively, if the grains are not perfect blackbodies, the disk radii would move further outward. It is possible that the then-unknown binary nature of HD 143811 AB may affect these inferred disk radii as well. In particular, this will set whether the cold debris belt is between the stellar binary (~ 0.2 au) and the exoplanet’s orbit (~ 64 au), or exterior to the planet’s orbit.

5.3. Sco-Cen Membership

The rotation and metallicity of these stars are generally consistent with Sco-Cen, as expected. We find relatively low $v \sin(i)$ for both A and B: 6.8 ± 0.6 and 2.9 ± 1.2 , respectively. Compared to other Sco-Cen stars of similar $B - V$ color

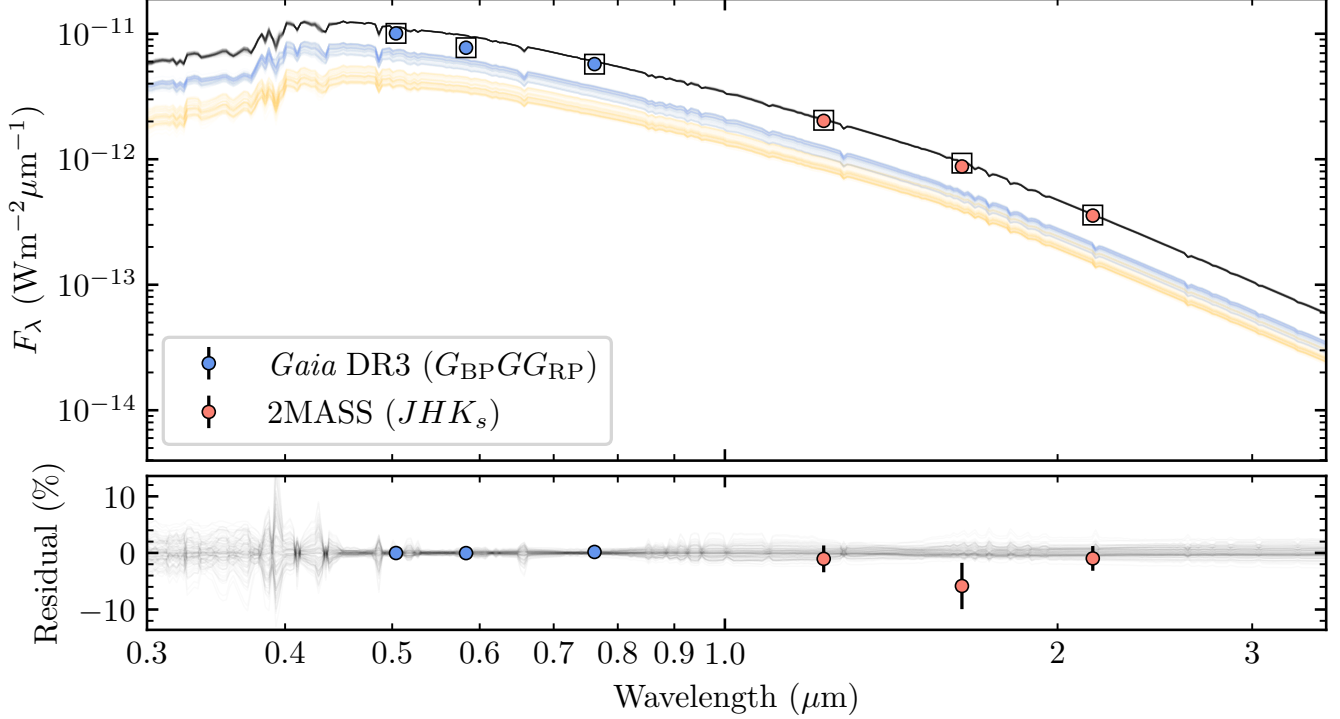


Figure 4. The results of a two-star fit to the unresolved optical and near-infrared photometry of the system from *Gaia* and 2MASS. Plotted are the spectral energy distribution of the blended system (black) and the two components (blue, yellow) drawn from the posterior distributions estimated using MCMC. Also shown are the synthetic photometry of the blended system derived from the median SED (black squares), and the observed photometry (circles).

from [A. Grandjean et al. \(2023\)](#) (their Figure 1b), these values are at the low end of their HARPS Sco-Cen sample, which span $v \sin(i)$ from ~ 3 to ~ 100 km/s. It is possible the two components of HD 143811 AB are being viewed more pole-on compared to other Sco-Cen members, or that tidal forces affected their rotational evolution. Slower overall rotation would be consistent with the lack of strong calcium emission we observe in the spectra. Our derived metallicity for the system from the spectral fit, -0.18 ± 0.10 , is within the distribution of 0.0 ± 0.18 measured by [A. Grandjean et al. \(2023\)](#).

The system radial velocity of $RV_0 = 0.48 \pm 0.02$ km/s, obtained from our orbit fit, is $\sim 1\sigma$ lower than the *Gaia* DR2 velocity of 1.68 ± 0.96 km/s, and significantly higher than the [C. H. Chen et al. \(2011\)](#) value of -11.3 ± 0.3 km/s. This large difference is to be expected given the semi-amplitude of each component of ~ 25 km/s. By combining our system radial velocity with *Gaia* DR3 astrometry we find space motions of the HD 143811 AB system of $(U, V, W) = (-2.68 \pm 0.04, -18.10 \pm 0.05, -4.68 \pm 0.02)$. This places HD 143811 AB $(2.1, 1.1, 0.9)\sigma$ from the central UVW of Upper Sco, as given by [N. J. Wright & E. E. Mamajek \(2018\)](#). The same calculation places the system slightly further from the central UVW of UCL, also from [N. J. Wright & E. E. Mamajek \(2018\)](#): $(1.6, 2.6, 0.9)\sigma$. This is in line with the BANYAN Σ results, when we combine *Gaia* DR3 astrometry with our radial velocity we find 72.1% probability of Upper Sco membership, 27.8% for UCL, and 0.2% for the field. The SED fit seems generally more consistent with UCL than Upper Sco, with the $20.9^{+1.8}_{-1.7}$ Myr age from that fit closer to the ~ 16 Myr UCL than the ~ 10 Myr Upper Sco. Similarly, a lower value of extinction (which would bring the SED and spectral fit temperatures more in line with each other) would also suggest UCL membership. Going forward, better age constraints on HD 143811 AB will allow for a more definitive determination of subgroup membership.

It is also interesting to compare HD 143811 AB b to another Sco-Cen directly imaged planet: HD 95086 b ([J. Rameau et al. 2013](#)). Both planets formed in the same association, are about the same age, orbit at roughly the same distance (~ 60 au), and are about the same mass ($\sim 5 M_{\text{Jup}}$). The major difference is the host star: HD 95086 is a $\sim 1.6 M_{\odot}$ A8 single star, while HD 143811 AB is a close binary containing a $1.30 M_{\odot}$ mid-F star and a $1.15 M_{\odot}$ late-F star. A key question is whether both planets formed at their present location, or if they moved outward after

formation, either from early interactions with the protoplanetary disk or due to gravitational scattering. Gravitational scattering is expected to play an important role in another Sco-Cen planet orbiting a tight binary, HD 106906 b (V. Bailey et al. 2014), which is at a projected separation of ~ 740 au. This very large separation is thought to result from gravitational interactions between the planet, the inner binary, and an additional Sco-Cen star that passed close to this system (R. J. De Rosa & P. Kalas 2019; M. M. Nguyen et al. 2021). If both HD 143811 AB b and HD 95086 b are close to their formation location it might suggest that wide-separation giant planet formation around close binary stars proceeds in a similar way as around single stars. The role of gravitational scattering can be tested with future orbit monitoring of the planet. In particular, if HD 143811 AB b has a more eccentric orbit than most directly imaged planets (B. P. Bowler et al. 2020) a scattering event might be more likely compared to in-situ formation. Further analysis of the binary orbit of HD 143811 AB, in particular the extent to which it is aligned (or not aligned) with the planet’s orbit, will also provide dynamical constraints on the origins of HD 143811 AB b.

With the current data it is not yet possible to robustly determine if the three-dimensional orbits of both the inner stellar binary and the outer planet are coplanar. In particular, the radial velocity data on the stellar binary provides no information on the position angle of nodes of the inner orbit. Similarly, with only a few degrees of orbital motion, the planet’s position angle of nodes is not well-determined, where despite four peaks in the posterior there is non-zero probability for all values between 0 and 360° (N. Jones et al. 2025, submitted ApJL). Without inclination angle and position angle of nodes measurements for both orbits, mutual inclination cannot be directly computed. Nevertheless, coplanarity cannot be ruled out with the current observations, with a model-dependent inclination angle of the binary orbit of $i_{AB} = 22.8^{+0.3}_{-0.2}^\circ$, and an inclination angle for the planet’s orbit of $i_b = 38 \pm 17^\circ$ (N. Jones et al. 2025, submitted ApJL). Thus, both inclination angle posteriors overlap at the $\sim 1\sigma$ level. Retrograde orbits are still possible, however, if $i_{AB} \approx 156$ is the actual inclination of the stellar binary. Additional orbital monitoring of the planet will allow a more precise inclination angle measurement and a quantitative comparison of the two inclination angles (e.g. G. M. Kennedy et al. 2013). Measurements of both orbits’ position angles of nodes, which for the inner binary would likely require VLTI/GRAVITY or *Gaia* DR4, would allow for a more direct test of coplanarity.

6. CONCLUSIONS

We report the characterization of the HD 143811 AB binary, the host of the directly imaged planet HD 143811 AB b. We extract RVs of both components from archival spectra at 22 epochs and derive orbital parameters, consistent with an eccentric ~ 18 day orbit, and a mass ratio of ~ 0.9 . Combining with the age of the system, unresolved photometry, and evolutionary models we derive masses of $M_A = 1.30^{+0.03}_{-0.05} M_\odot$ and $M_B = 1.15^{+0.03}_{-0.04} M_\odot$ for the two components.

Future observations of the HD 143811 AB system will refine the orbital parameters of both orbits. While the RV orbit of HD 143811 AB is very well constrained, interferometry of the system will make it possible to resolve the ~ 1 mas visual orbit of the binary, and so directly measure the full 3D orbit. In addition, *Gaia* DR 4 will contain individual astrometric scans, which may have the precision to detect the ~ 0.1 mas photocenter orbit of the binary. Similarly, additional orbital monitoring of the planet will better constrain its 3D orbit, allowing a direct measurement of the mutual inclination of the two orbits. In addition to aiding 3-body modeling of the system, these improved orbits will place valuable constraints on the formation mechanism and dynamical evolution of this system.

An improved exoplanet orbit will be especially interesting when coupled with future long wavelength observations of the star, such as from JWST MRS. More accurately determining the debris disk’s radius and extent, especially given the physical parameters of the stellar binary, will better inform the dynamics of the disk, and its interactions with the planet.

HD 143811 AB b joins a growing list of directly imaged planets in binary systems including 51 Eri b, B. Macintosh et al. (2015) and HD 106906 b V. Bailey et al. (2014); R. J. De Rosa & P. Kalas (2019). With additional detections, it will become feasible to determine how the occurrence rate of wide-separation giant planets depends on binary properties, and how it compares to the occurrence rate for single stars. This comparison has traditionally been difficult, given the relatively low occurrence rate of wide-separation giant planets and the tendency of imaging surveys to screen for binaries (e.g. M. Bonavita et al. 2016). Improvements to high contrast imaging, such as the upcoming Gemini Planet Imager 2.0 (J. Chilcote et al. 2024), will enable better sensitivity to giant planets orbiting single stars, orbiting one star in wide binaries, and orbiting both stars in close binaries. *Gaia* DR4 will also allow a comparison of closer-in giant planet populations between binaries and single stars, especially in cases where astrometry from both components of the binary can be extracted.

ACKNOWLEDGMENTS

Based on observations obtained at the international Gemini Observatory, a program of NSF NOIRLab, which is managed by the Association of Universities for Research in Astronomy (AURA) under a cooperative agreement with the U.S. National Science Foundation on behalf of the Gemini Observatory partnership: the U.S. National Science Foundation (United States), National Research Council (Canada), Agencia Nacional de Investigación y Desarrollo (Chile), Ministerio de Ciencia, Tecnología e Innovación (Argentina), Ministério da Ciência, Tecnologia, Inovações e Comunicações (Brazil), and Korea Astronomy and Space Science Institute (Republic of Korea).

This publication makes use of data products from the Two Micron All Sky Survey, which is a joint project of the University of Massachusetts and the Infrared Processing and Analysis Center/California Institute of Technology, funded by the National Aeronautics and Space Administration and the National Science Foundation

Based on observations collected at the European Organisation for Astronomical Research in the Southern Hemisphere under ESO programme(s) 0101.A-9012(A), 0107.A-9004(A), 0109.A-9014(A). This research has made use of the SIMBAD database, CDS, Strasbourg Astronomical Observatory, France. This research has made use of the VizieR catalogue access tool, CDS, Strasbourg Astronomical Observatory, France (DOI : 10.26093/cds/vizieR).

This work has made use of data from the European Space Agency (ESA) mission *Gaia* (<https://www.cosmos.esa.int/gaia>), processed by the Gaia Data Processing and Analysis Consortium (DPAC, <https://www.cosmos.esa.int/web/gaia/dpac/consortium>). Funding for the DPAC has been provided by national institutions, in particular the institutions participating in the *Gaia* Multilateral Agreement.

Based on observations obtained with the Apache Point Observatory 3.5-meter telescope, which is owned and operated by the Astrophysical Research Consortium.

A.E.P., W.R., E.L.N., and A.A. are supported by NASA grant 80NSSC21K0958 and NSF grant AST 2510959. E.L.N. and A.J.R.W.S. are supported by NASA grant 21-ADAP21-0130. B.L.L. acknowledges support from the National Science Foundation Astronomy & Astrophysics Postdoctoral Fellowship under Award No. 2401654. A.S. is supported by the National Science Foundation Graduate Research Fellowship under Grant No. 2139433. Any opinions, findings, and conclusions or recommendations expressed in this material are those of the author(s) and do not necessarily reflect the views of the National Science Foundation.

Facilities: *Gaia*, *Hipparcos*, *MaxPlanck* : 2.2m, ARC

Software: *astropy* (Astropy Collaboration et al. 2013, 2018, 2022), *SciPy* (P. Virtanen et al. 2020), *NumPy* (C. R. Harris et al. 2020), *emcee* (D. Foreman-Mackey et al. 2013)

APPENDIX

We investigate the accuracy of our stellar parameter spectral fit with a set of 10 well-studied F and G stars, with stellar parameters reported by C. Soubiran et al. (2022). We observed these stars (which were used as RV standards) with the Astronomy Research Consortium Echelle Spectrograph (ARCES) on the ARC 3.5 meter telescope at Apache Point Observatory between 2020 to 2025. ARCES is an $R \sim 35,000$ spectrograph with coverage from 3,200 Å to 10,000 Å (S.-i. Wang et al. 2003), similar to the $R \sim 48,000$ FEROS. These observations are reduced using the standard ARCES IRAF/PyRAF reduction pipeline provided by APO⁴³.

We use the spectral fitting method described above (modified to model a single star rather than an SB2) to extract the effective temperatures and metallicities of these 10 stars. The posteriors on these parameters are then compared to the measured values of C. Soubiran et al. (2022). We find that the $\log(g)$ values we extract from our method are significantly different from the literature values. This could be the result of the PHOENIX model grids being too coarsely sampled in $\log(g)$, our choice of lines not constraining $\log(g)$, or limitations in our science spectra such as the spectral resolution or continuum correction, all of which could prevent our method from constraining $\log(g)$. Since gravity is covariant with metallicity and temperature, we place a prior on $\log(g)$, rather than attempt to measure it from our spectral fits. We use a prior for each star of a Gaussian, from the value and error reported by C. Soubiran et al. (2022).

⁴³ <http://astronomy.nmsu.edu/apo-wiki/doku.php?id=arces>

Our measured effective temperatures and metallicities for these ten stars are shown in Figure 5. The residuals show no systematic offset from the literature values for temperature or metallicity. The residuals in effective temperature have a median of -10 K and a standard deviation of 69 K, while the metallicity residuals have a median of 0.017 dex and a standard deviation of 0.055 dex. To ensure we are not underestimating uncertainties on temperature and metallicity, we add 56.9 K and 0.052 dex in quadrature to our measured temperature and metallicity uncertainties. This brings the reduced χ^2 between C. Soubiran et al. (2022) and our values to 1.

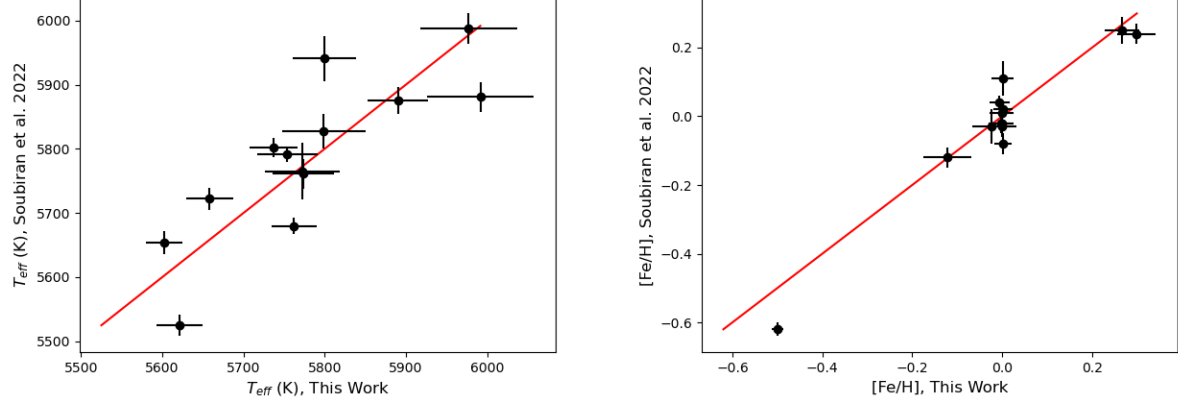


Figure 5. We are able to accurately recover effective temperature and metallicity when applying our method to well-characterized F and G stars. A comparison of literature measurements from C. Soubiran et al. (2022) and our spectral fitting method applied to these same stars observed with APO/ARCES shows good agreement, with no systematic offset.

REFERENCES

- Astropy Collaboration, Robitaille, T. P., Tollerud, E. J., et al. 2013, *A&A*, 558, A33, doi: [10.1051/0004-6361/201322068](https://doi.org/10.1051/0004-6361/201322068)
- Astropy Collaboration, Price-Whelan, A. M., Sipőcz, B. M., et al. 2018, *AJ*, 156, 123, doi: [10.3847/1538-3881/aabc4f](https://doi.org/10.3847/1538-3881/aabc4f)
- Astropy Collaboration, Price-Whelan, A. M., Lim, P. L., et al. 2022, *ApJ*, 935, 167, doi: [10.3847/1538-4357/ac7c74](https://doi.org/10.3847/1538-4357/ac7c74)
- Bailey, V., Meshkat, T., Reiter, M., et al. 2014, *ApJL*, 780, L4, doi: [10.1088/2041-8205/780/1/L4](https://doi.org/10.1088/2041-8205/780/1/L4)
- Ballerín, N. P., Rieke, G. H., Su, K. Y. L., & Montiel, E. 2013, *ApJ*, 775, 55, doi: [10.1088/0004-637X/775/1/55](https://doi.org/10.1088/0004-637X/775/1/55)
- Baraffe, I., Homeier, D., Allard, F., & Chabrier, G. 2015, *A&A*, 577, A42, doi: [10.1051/0004-6361/201425481](https://doi.org/10.1051/0004-6361/201425481)
- Bonavita, M., Desidera, S., Thalmann, C., et al. 2016, *A&A*, 593, A38, doi: [10.1051/0004-6361/201628231](https://doi.org/10.1051/0004-6361/201628231)
- Bowler, B. P., Blunt, S. C., & Nielsen, E. L. 2020, *AJ*, 159, 63, doi: [10.3847/1538-3881/ab5b11](https://doi.org/10.3847/1538-3881/ab5b11)
- Castelli, F., & Kurucz, R. L. 2003, in *IAU Symposium*, Vol. 210, *Modelling of Stellar Atmospheres*, ed. N. Piskunov, W. W. Weiss, & D. F. Gray, A20, doi: [10.48550/arXiv.astro-ph/0405087](https://doi.org/10.48550/arXiv.astro-ph/0405087)
- Cheetham, A., Ségransan, D., Peretti, S., et al. 2018, *A&A*, 614, A16, doi: [10.1051/0004-6361/201630136](https://doi.org/10.1051/0004-6361/201630136)
- Chen, C. H., Mamajek, E. E., Bitner, M. A., et al. 2011, *ApJ*, 738, 122, doi: [10.1088/0004-637X/738/2/122](https://doi.org/10.1088/0004-637X/738/2/122)
- Chen, C. H., Mittal, T., Kuchner, M., et al. 2014, *ApJS*, 211, 25, doi: [10.1088/0067-0049/211/2/25](https://doi.org/10.1088/0067-0049/211/2/25)
- Chilcote, J., Konopacky, Q., Hamper, R., et al. 2024, in *Society of Photo-Optical Instrumentation Engineers (SPIE) Conference Series*, Vol. 13096, *Ground-based and Airborne Instrumentation for Astronomy X*, ed. J. J. Bryant, K. Motohara, & J. R. D. Vernet, 1309699, doi: [10.1117/12.3020642](https://doi.org/10.1117/12.3020642)
- Choi, J., Dotter, A., Conroy, C., et al. 2016, *ApJ*, 823, 102, doi: [10.3847/0004-637X/823/2/102](https://doi.org/10.3847/0004-637X/823/2/102)
- Cotten, T. H., & Song, I. 2016, *ApJS*, 225, 15, doi: [10.3847/0067-0049/225/1/15](https://doi.org/10.3847/0067-0049/225/1/15)
- de Geus, E. J., de Zeeuw, P. T., & Lub, J. 1989, *A&A*, 216, 44
- De Rosa, R. J., & Kalas, P. 2019, *AJ*, 157, 125, doi: [10.3847/1538-3881/ab0109](https://doi.org/10.3847/1538-3881/ab0109)
- De Rosa, R. J., Nielsen, E. L., Blunt, S. C., et al. 2015, *ApJL*, 814, L3, doi: [10.1088/2041-8205/814/1/L3](https://doi.org/10.1088/2041-8205/814/1/L3)
- de Zeeuw, P. T., Hoogerwerf, R., de Bruijne, J. H. J., Brown, A. G. A., & Blaauw, A. 1999, *AJ*, 117, 354, doi: [10.1086/300682](https://doi.org/10.1086/300682)

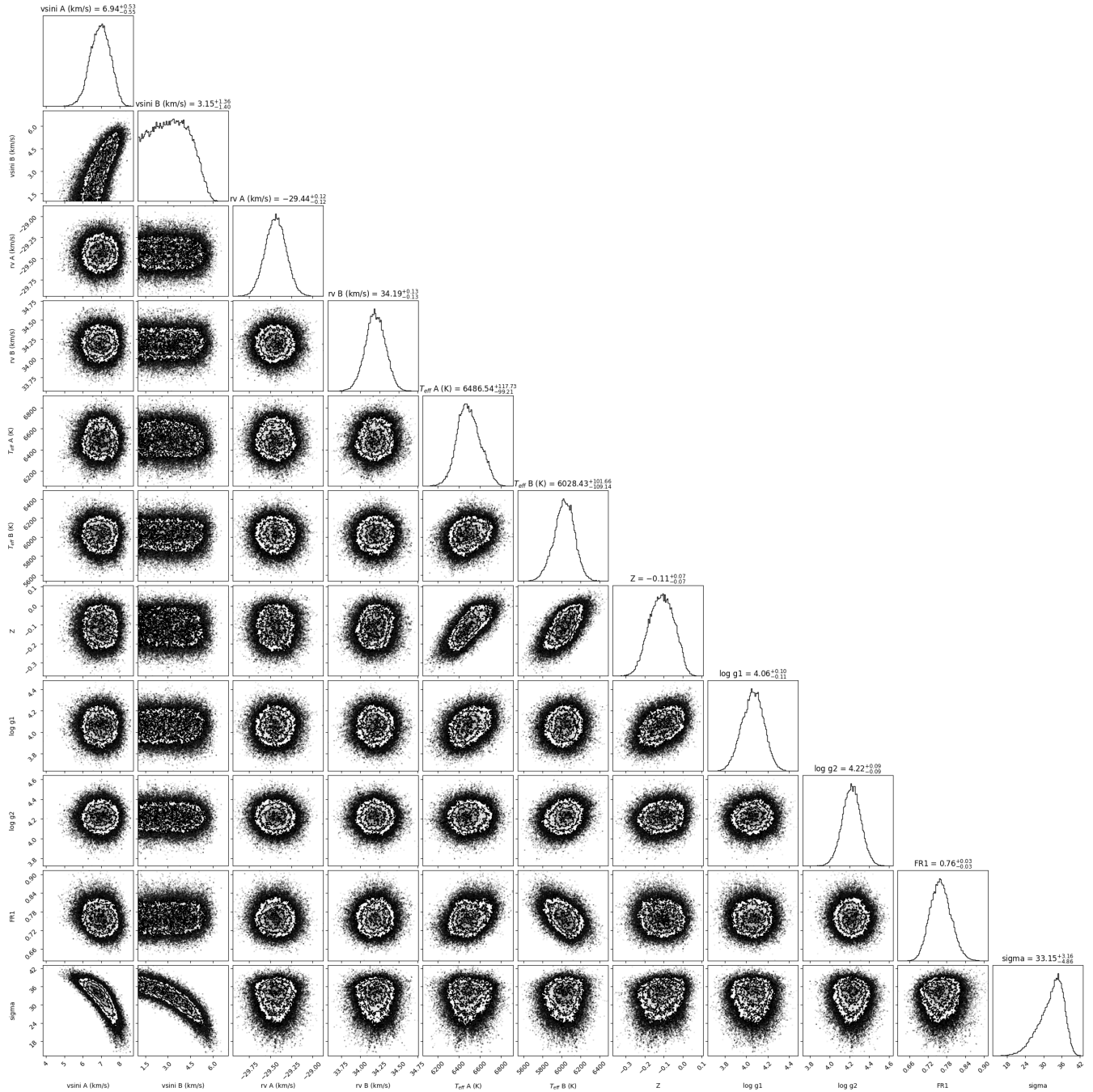


Figure 6. The posterior distribution for the binary fit to the 2018-04-18 FEROS spectrum, fitting for stellar parameters and radial velocities of both components of the binary.

Dotter, A. 2016, *ApJS*, 222, 8,

doi: [10.3847/0067-0049/222/1/8](https://doi.org/10.3847/0067-0049/222/1/8)

Duquennoy, A., & Mayor, M. 1991, *A&A*, 248, 485

Foreman-Mackey, D., Hogg, D. W., Lang, D., & Goodman, J. 2013, *PASP*, 125, 306, doi: [10.1086/670067](https://doi.org/10.1086/670067)

Gagné, J., Mamajek, E. E., Malo, L., et al. 2018, *ApJ*, 856, 23, doi: [10.3847/1538-4357/aaae09](https://doi.org/10.3847/1538-4357/aaae09)

Gaia Collaboration, Brown, A. G. A., Vallenari, A., et al.

2018, *A&A*, 616, A1, doi: [10.1051/0004-6361/201833051](https://doi.org/10.1051/0004-6361/201833051)

Gaia Collaboration, Vallenari, A., Brown, A. G. A., et al.

2023, *A&A*, 674, A1, doi: [10.1051/0004-6361/202243940](https://doi.org/10.1051/0004-6361/202243940)

Galli, P. A. B., Joncour, I., & Moraux, E. 2018, *MNRAS*, 477, L50, doi: [10.1093/mnras/sly036](https://doi.org/10.1093/mnras/sly036)

Grandjean, A., Lagrange, A. M., Meunier, N., et al. 2023, *A&A*, 669, A12, doi: [10.1051/0004-6361/202141235](https://doi.org/10.1051/0004-6361/202141235)

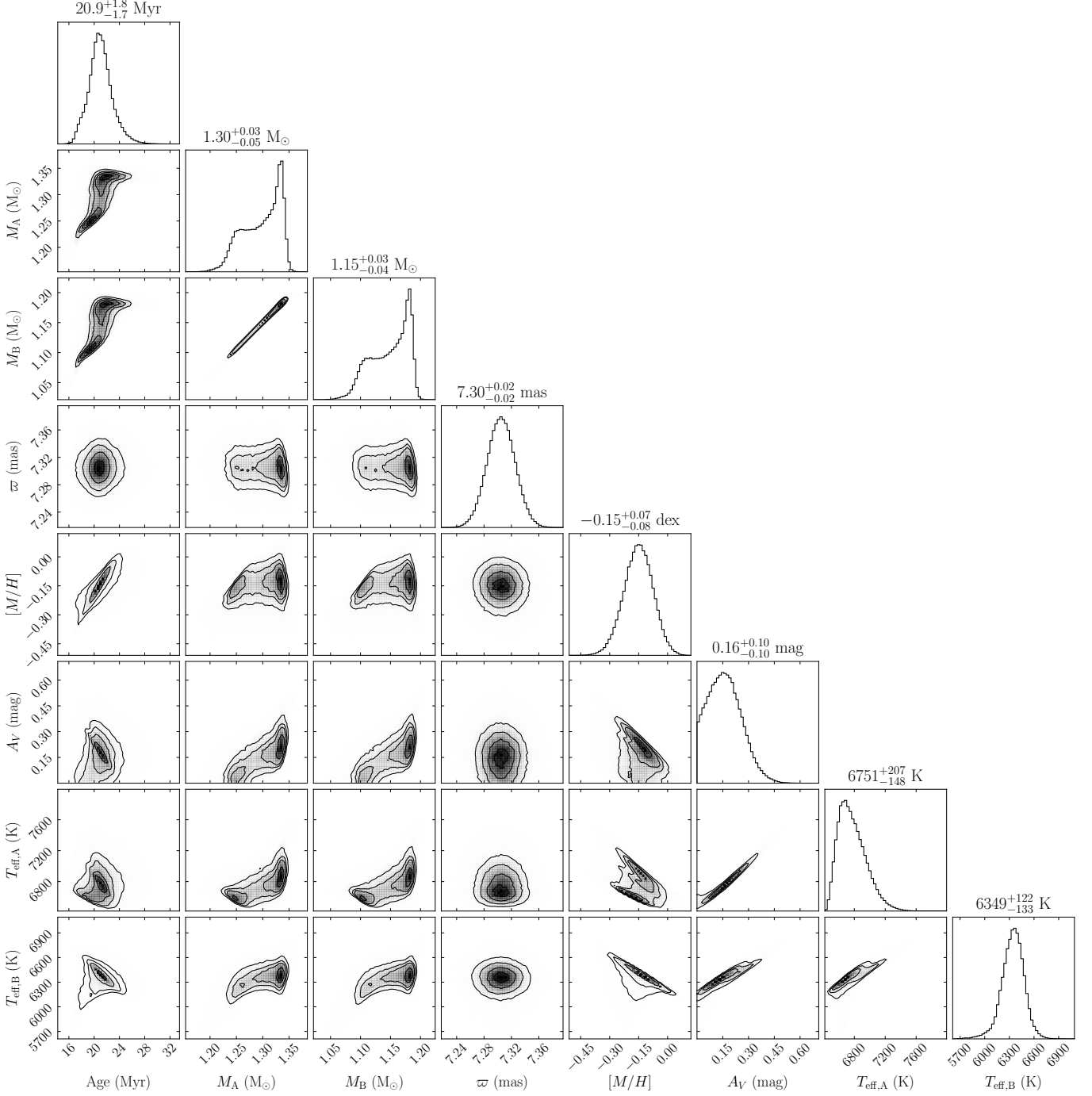


Figure 7. The posterior distribution for the two-star fit to the unresolved photometric measurements, giving the six fitted parameters and their covariances. The effective temperature, a derived parameter, of both components is also shown.

GRAVITY Collaboration, Abuter, R., Accardo, M., et al. 2017, *A&A*, 602, A94, doi: [10.1051/0004-6361/201730838](https://doi.org/10.1051/0004-6361/201730838)

Harris, C. R., Millman, K. J., van der Walt, S. J., et al. 2020, *Nature*, 585, 357, doi: [10.1038/s41586-020-2649-2](https://doi.org/10.1038/s41586-020-2649-2)

Hauschildt, P. H., & Baron, E. 1999, *Journal of Computational and Applied Mathematics*, 109, 41, doi: [10.48550/arXiv.astro-ph/9808182](https://doi.org/10.48550/arXiv.astro-ph/9808182)

Husser, T. O., Wende-von Berg, S., Dreizler, S., et al. 2013, *A&A*, 553, A6, doi: [10.1051/0004-6361/201219058](https://doi.org/10.1051/0004-6361/201219058)

Jang-Condell, H., Chen, C. H., Mittal, T., et al. 2015, *ApJ*, 808, 167, doi: [10.1088/0004-637X/808/2/167](https://doi.org/10.1088/0004-637X/808/2/167)

Johnson, J. A., Aller, K. M., Howard, A. W., & Crepp, J. R. 2010, *PASP*, 122, 905, doi: [10.1086/655775](https://doi.org/10.1086/655775)

- Kaufer, A., Stahl, O., Tubbesing, S., et al. 1999, *The Messenger*, 95, 8
- Kennedy, G. M., Wyatt, M. C., Bryden, G., Wittenmyer, R., & Sibthorpe, B. 2013, *MNRAS*, 436, 898, doi: [10.1093/mnras/stt1657](https://doi.org/10.1093/mnras/stt1657)
- Kraus, A. L., Ireland, M. J., Huber, D., Mann, A. W., & Dupuy, T. J. 2016, *AJ*, 152, 8, doi: [10.3847/0004-6256/152/1/8](https://doi.org/10.3847/0004-6256/152/1/8)
- Lagrange, A. M., Bonnefoy, M., Chauvin, G., et al. 2010, *Science*, 329, 57, doi: [10.1126/science.1187187](https://doi.org/10.1126/science.1187187)
- Luhman, K. L., & Eskin, T. L. 2020, *AJ*, 160, 44, doi: [10.3847/1538-3881/ab9599](https://doi.org/10.3847/1538-3881/ab9599)
- Macintosh, B., Graham, J. R., Barman, T., et al. 2015, *Science*, 350, 64, doi: [10.1126/science.aac5891](https://doi.org/10.1126/science.aac5891)
- McDonald, I., Zijlstra, A. A., & Boyer, M. L. 2012, *MNRAS*, 427, 343, doi: [10.1111/j.1365-2966.2012.21873.x](https://doi.org/10.1111/j.1365-2966.2012.21873.x)
- Nguyen, M. M., De Rosa, R. J., & Kalas, P. 2021, *AJ*, 161, 22, doi: [10.3847/1538-3881/abc012](https://doi.org/10.3847/1538-3881/abc012)
- Nielsen, E. L., Liu, M. C., Wahhaj, Z., et al. 2013, *ApJ*, 776, 4, doi: [10.1088/0004-637X/776/1/4](https://doi.org/10.1088/0004-637X/776/1/4)
- Nielsen, E. L., De Rosa, R. J., Macintosh, B., et al. 2019, *AJ*, 158, 13, doi: [10.3847/1538-3881/ab16e9](https://doi.org/10.3847/1538-3881/ab16e9)
- Nielsen, E. L., De Rosa, R. J., Wang, J. J., et al. 2020, *AJ*, 159, 71, doi: [10.3847/1538-3881/ab5b92](https://doi.org/10.3847/1538-3881/ab5b92)
- Pecaut, M. J., & Mamajek, E. E. 2016, *MNRAS*, 461, 794, doi: [10.1093/mnras/stw1300](https://doi.org/10.1093/mnras/stw1300)
- Pecaut, M. J., Mamajek, E. E., & Bubar, E. J. 2012, *ApJ*, 746, 154, doi: [10.1088/0004-637X/746/2/154](https://doi.org/10.1088/0004-637X/746/2/154)
- Raghavan, D., McAlister, H. A., Henry, T. J., et al. 2010, *ApJS*, 190, 1, doi: [10.1088/0067-0049/190/1/1](https://doi.org/10.1088/0067-0049/190/1/1)
- Rameau, J., Chauvin, G., Lagrange, A. M., et al. 2013, *ApJL*, 772, L15, doi: [10.1088/2041-8205/772/2/L15](https://doi.org/10.1088/2041-8205/772/2/L15)
- Skrutskie, M. F., Cutri, R. M., Stiening, R., et al. 2006, *AJ*, 131, 1163, doi: [10.1086/498708](https://doi.org/10.1086/498708)
- Soubiran, C., Brouillet, N., & Casamiquela, L. 2022, *A&A*, 663, A4, doi: [10.1051/0004-6361/202142409](https://doi.org/10.1051/0004-6361/202142409)
- Torres, G., Latham, D. W., & Quinn, S. N. 2021, *ApJ*, 921, 117, doi: [10.3847/1538-4357/ac1585](https://doi.org/10.3847/1538-4357/ac1585)
- Virtanen, P., Gommers, R., Oliphant, T. E., et al. 2020, *Nature Methods*, 17, 261, doi: [10.1038/s41592-019-0686-2](https://doi.org/10.1038/s41592-019-0686-2)
- Wang, S.-i., Hildebrand, R. H., Hobbs, L. M., et al. 2003, in *Society of Photo-Optical Instrumentation Engineers (SPIE) Conference Series*, Vol. 4841, *Instrument Design and Performance for Optical/Infrared Ground-based Telescopes*, ed. M. Iye & A. F. M. Moorwood, 1145–1156, doi: [10.1117/12.461447](https://doi.org/10.1117/12.461447)
- Wright, E. L., Eisenhardt, P. R. M., Mainzer, A. K., et al. 2010, *AJ*, 140, 1868, doi: [10.1088/0004-6256/140/6/1868](https://doi.org/10.1088/0004-6256/140/6/1868)
- Wright, N. J., & Mamajek, E. E. 2018, *MNRAS*, 476, 381, doi: [10.1093/mnras/sty207](https://doi.org/10.1093/mnras/sty207)
- Zakhzhay, O. V., Launhardt, R., Müller, A., et al. 2022, *A&A*, 667, A63, doi: [10.1051/0004-6361/202244213](https://doi.org/10.1051/0004-6361/202244213)